

Soil production limits and the transition to bedrock-dominated landscapes

Arjun M. Heimsath^{1*}, Roman A. DiBiase^{1†} and Kelin X. Whipple¹

The extent and persistence of the Earth's soil cover depends on the long-term balance between soil production and erosion. Higher soil production rates under thinner soils provide a critical stabilizing feedback mechanism^{1–3}, and climate- and lithology-controlled soil production is thought to set the upper limit for steady-state hillslope erosion⁴. In this framework, erosion rates exceeding the maximum soil production rate can be due only to bedrock mass wasting⁵. However, observation of pervasive, if patchy, soil cover in areas of rugged topography and rapid erosion indicates additional stabilizing mechanisms. Here we present ¹⁰Be-derived estimates of soil-production and detrital erosion rates that show that soil production rates increase with increasing catchment-averaged erosion rates, a feedback that enhances soil-cover persistence. We show that a process transition to landslide-dominated erosion in steeper, more rapidly eroding catchments results in thinner, patchier soils and rockier topography, but find that there is no sudden transition to bedrock landscapes. Instead, using our global data compilation, we suggest that soil production may increase in frequency and magnitude to keep up with increasing erosion rates. We therefore conclude that existing models^{6–8} greatly exaggerate changes in critical-zone processes in response to tectonic uplift.

Soil is critical to most terrestrial ecosystems, surface water hydrology and the function of life-sustaining biogeochemical cycles⁹. Predicting what drives the transition between soil-mantled and rocky landscapes may, therefore, be the most profound challenge for landscape evolution and critical-zone studies. Despite its fundamental importance, this transition has not been studied systematically. Here we focus on upland, colluvial soils and present a new data set of 58 soil production rates (SPRs) quantified from ¹⁰Be concentrations in soil pits across the San Gabriel Mountains (SGM) of California: from catchments spanning two orders of magnitude in erosion rate as the landscape varies from gentle, soil mantled and creep dominated in the west to steep, rocky and landslide dominated in the east¹⁰. These rates are the first to cross the transition from soil-mantled to rocky hillslopes. They clearly document local SPRs in steep, rapidly eroding terrain that greatly exceed the maximum SPR (SP_{max}) determined for low-relief, soil-mantled areas with similar climate and lithology. Combined with a global compilation of published SPRs, these new data enable us to examine in detail how the soil mantle and the soil production process respond to increasing erosion rates and the associated transition to erosion by episodic landslides. We complement this interrogation of process rates with analysis of high-resolution light detection and ranging (LiDAR) topographic data and adapt a numerical model¹¹ to explore the role of episodic landslides in the gradual transition from soil-mantled to bedrock-dominated landscapes.

The SGM are a steep, active range in southern California, bounded to the north by the strike-slip San Andreas Fault and to the south by the Sierra Madre–Cucamonga thrust system. Agreement among long-term exhumation rates¹², millennial erosion rates¹⁰ and Holocene slip rates¹³ along the southern range front indicates active uplift and erosion of the range for at least the past 5 Myr. Furthermore, along-strike variations in rock uplift have created a strong west–east gradient in erosion rates and consequent west–east gradients in hillslope angles, channel steepness and topographic relief (Fig. 1). DiBiase *et al.*¹⁰ exploited these gradients and used cosmogenic ¹⁰Be concentrations from detrital sands in 50 catchments (<1–175 km²) to quantify how catchment-averaged erosion rates change with mean hillslope angle. Average erosion rates increase steadily with increasing slope from 35 to ~200 m Myr⁻¹, where slopes reach their threshold. At rates above ~200 m Myr⁻¹, slopes are insensitive to further increases in erosion rate driven by relative base-level fall (Fig. 1e), corroborating recent analyses from other landscapes^{14,15}. Field observations indicate that this transition in hillslope form is associated with a transition from steady, creep-related processes to stochastic mass wasting in all three landscapes^{10,14,15}. Furthermore, in the SGM and nearby San Bernardino Mountains, recent studies observed that hillslopes are rockier where erosion is dominated by mass-wasting processes^{10,15}.

The predicted transition to threshold hillslope gradients at relatively low erosion rates due to limits of soil-creep transport rates and substrate weaknesses leading to mass wasting is now well documented^{10,14,16–19}. Although the role of soil production in steep landscapes was not directly constrained, the transition to threshold slopes often corresponds with erosion rates (E) of about 200 m Myr⁻¹ (Fig. 1e)^{10,14–16}, roughly matching an estimated SP_{max} (ref. 8,10,20). We emphasize, however, that the transition to mass-wasting processes and slope-invariant erosion rates will also arise in landscapes developed entirely on unconsolidated sediments, and thus will occur even without a SPR limitation. Indeed, the relationship between mean hillslope gradient and erosion rate is well explained by a nonlinear soil transport model²¹, assuming no SPR limitation^{10,14}. Two interesting questions emerge. First, can a process transition to landslides explain patchy soil cover? Second, is SP_{max} invariant with E as generally believed, or does it increase with E and help maintain soil cover?

To address the first question, we expand on our field observations of relative bedrock exposure as a function of topography and erosion rate with an analysis of a LiDAR-derived, high-resolution (1 m grid) digital elevation model (DEM; Fig. 1a). For each of our detrital cosmogenic sample catchments within the LiDAR coverage, we extracted a slope-based rock exposure index (REI), which we calibrated to independently mapped bedrock outcrops using high-resolution panoramic photographs²². Figure 1b–d shows three representative landscape elements highlighting areas that

¹School of Earth and Space Exploration, Arizona State University, Tempe, Arizona 85287, USA. [†]Present address: Division of Geological and Planetary Sciences, California Institute of Technology, Pasadena, California 91125, USA. *e-mail: Arjun.Heimsath@asu.edu.

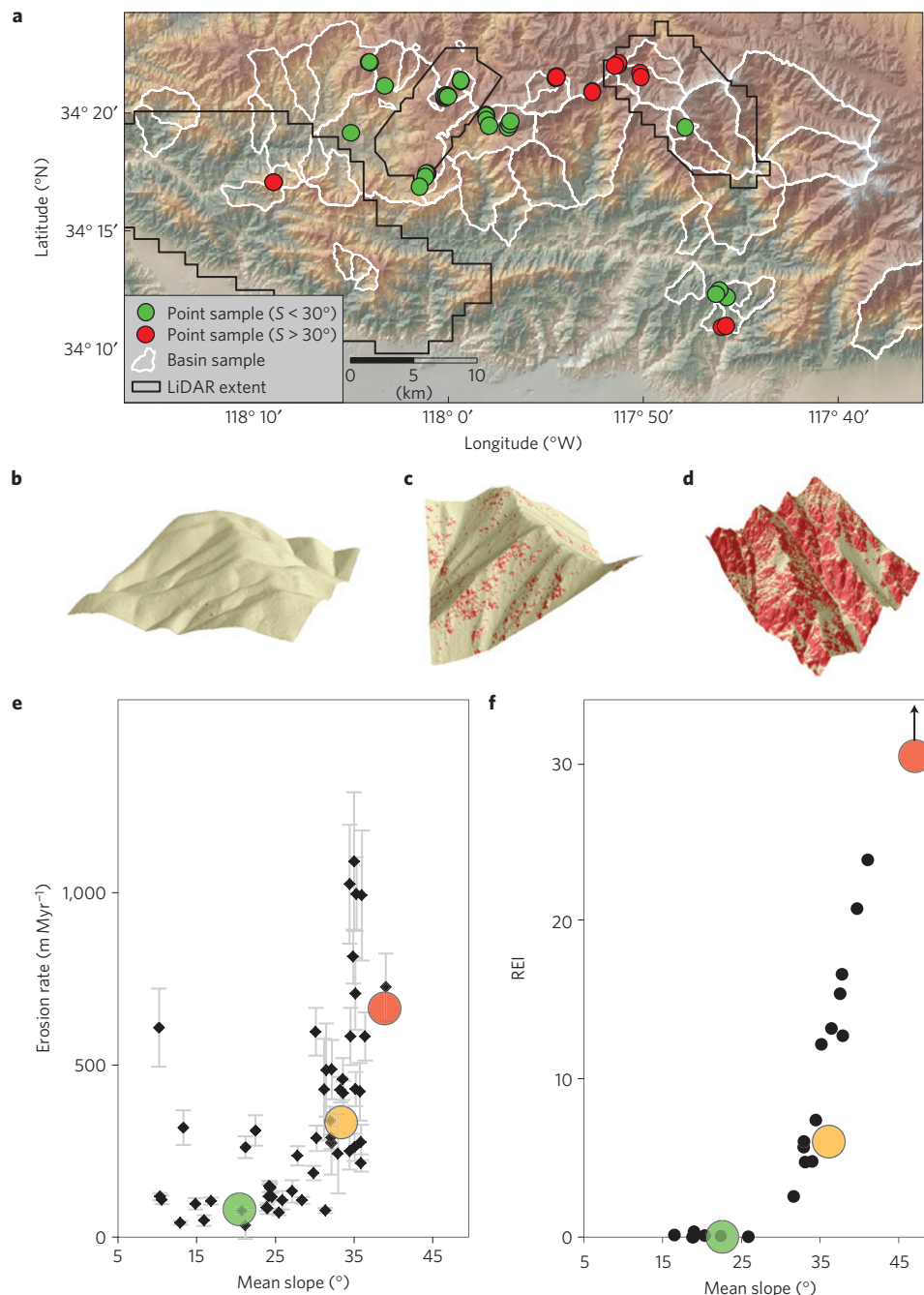


Figure 1 | San Gabriel Mountains, California. **a**, Elevation (0–3,000 m) over shaded relief. Circles show SPR sample locations. White outlines are detrital CRN erosion catchments¹⁰. Black outlines indicate LiDAR coverage²². **b–d**, Representative (20 ha) surfaces for convex (**b**), planar (**c**) and rocky (**d**) hillslopes. Red pixels indicate exposed bedrock by REI. **e**, Catchment erosion rates plotted against mean slope¹⁰. Error bars show 1σ analytical uncertainty. **f**, REI of catchments within LiDAR coverage plotted against mean slope measured from 1 m DEM. Green, yellow and red circles in **e** and **f** show representative hillslope elements **b**, **c** and **d**, respectively.

the REI attributes to be associated outcropping bedrock. Convex, soil-mantled hillslopes are low gradient, and have little to no exposed bedrock (Fig. 1b). Steep, planar hillslopes tend to have a thin (≤ 20 cm) but continuous mantle of soil and scree with little outcropping bedrock (Fig. 1c). Conversely, rugged, threshold slopes have substantial amounts of exposed rock, and show an increasing fraction of areas with locally extreme slopes (Fig. 1d). Our sampled catchments typically include a range of hillslope styles. The linear increase of REI with slopes exceeding 30° ($R^2 = 0.95$) reflects increasing bedrock dominance in steep basins and coincides with the transition to landslides and threshold hillslopes¹⁶ (Fig. 1f).

REI, and thus the amount of exposed rock, increases with mean slope, but many of our catchments previously interpreted to be landslide dominated because of high erosion rates and threshold slopes have a surprisingly continuous soil mantle. To investigate the impact of episodic mass wasting on the preservation of a soil mantle, we adapted a stochastic landsliding model originally developed for testing the validity of the detrital cosmogenic radionuclide (CRN) method in such areas^{11,23}. These models assume that hillslope erosion occurs at a background rate ($< SP_{\max}$) augmented by mass wasting, with landslide frequency and depth determining the difference between the background (soil production) rate

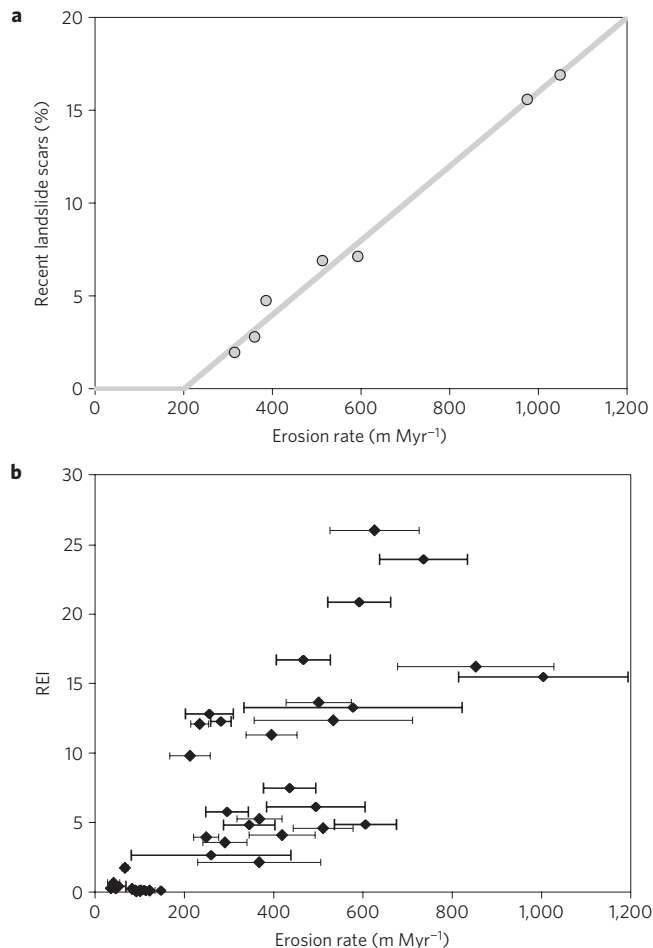


Figure 2 | Landscape model and REI versus erosion rate. **a**, Percentage of landscape covered by recent (<1,000 years) landslide scars as a function of modelled erosion rate. Circles indicate individual model runs, with a best-fit line shown in grey. No landslide scars expected below 'background' erosion rate of 200 m Myr⁻¹. **b**, REI plotted against detrital CRN erosion rates for catchments within LiDAR coverage. Error bars as in Fig. 1e.

and E . By assuming a SPR of 200 m Myr⁻¹ (ref. 9), and using landslide size distributions from the SGM (ref. 24), we find that a significant soil mantle (>80%) is retained even when landsliding rates exceed the model SPR by a factor of 4 (Fig. 2 and Supplementary Information). When we plot our REI against erosion rate for catchments with CRN-derived erosion rates (Fig. 2b), two groupings of catchments stand out amidst the scatter. Below erosion rates of ~ 200 m Myr⁻¹, catchments are nearly entirely smooth (soil mantled), and above ~ 200 m Myr⁻¹, catchments show significantly higher REI values, corresponding to observations of more exposed bedrock. Comparison with model results indicates that a high SPR is apparently not needed to explain our observation of pervasive, if patchy, soil in steep regions of the SGM. It may be that soil cover is far more extensive in steep, rapidly eroding topography than previously predicted.

Addressing the second question, whether SP_{\max} is invariant with catchment erosion rate or not, requires quantifying SPRs from soil-mantled to rocky landscapes. To do so, we measured *in situ*-produced ¹⁰Be concentrations from in-place saprolite samples spanning the study area (Fig. 1). Soil thickness increases systematically downslope and with decreasing hillslope convexity across the soil-dominated regions of the field area. Samples collected across this more slowly eroding, convex-up part of the landscape define a robust soil-production function, with SP_{\max}

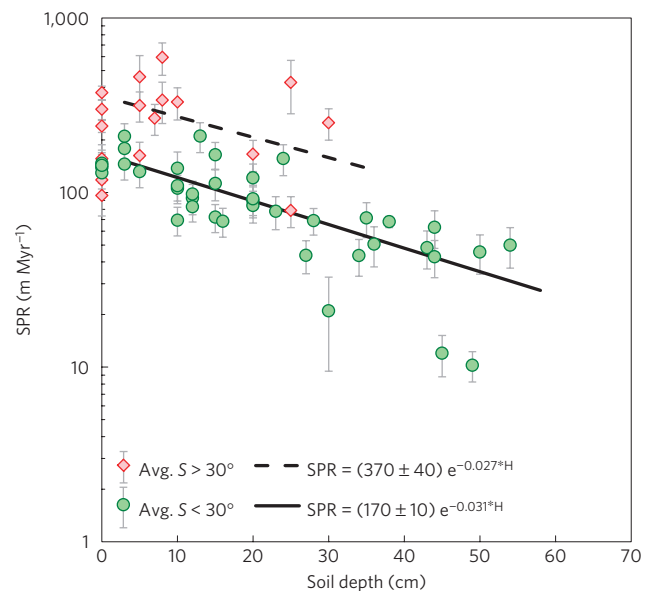


Figure 3 | SGM soil-production functions. SPRs plotted against soil thickness. Green circles from gentle landscape samples with minimal to no bedrock outcropping and smoothly convex-up ridges. Red diamonds from steep landscape where side slopes become planar and dominant erosional process transitions to landsliding. Solid line shows variance-weighted fit to low-slope samples, excluding zero depths, defining function for SPRs from soil thickness, H . Eleven samples from beneath shallow soils from steep landscapes yields variance-weighted soil-production function with significantly higher SP_{\max} (dashed line). See Supplementary Information for data table and more detailed methods.

equalling 170 ± 10 m Myr⁻¹ (Fig. 3). As morphology shifts from convex-up to planar (Fig. 1b,c), slope gradients increase and we observed the soil mantle transition from being ubiquitous to becoming increasingly patchy. We focused sampling of steep (average slope >30°) hillslopes on smooth, locally divergent ridges away from any landslide scars, thus ensuring that our ¹⁰Be concentrations represent SPRs (see Supplementary Information). Importantly, we observed that soil patches on threshold slopes, although typically thin (<20 cm) and coarse grained, are clearly produced locally and are not colluvial accumulations. SPRs from saprolite under these thin to non-existent soils are among the highest such rates ever reported, and exceed SP_{\max} predicted from the low-relief soil pits by up to a factor of four, with a predicted maximum rate of 370 ± 40 (Fig. 3).

These high SPRs directly contradict the existing paradigm for soil-mantled landscapes, which indicates that SP_{\max} is constant for a given climate and lithology, and that landscapes are faced with a stark choice: either erode slowly beneath a protective soil cloak or become barren bedrock when SP_{\max} is exceeded. According to the previous paradigm, high SPRs cannot exist (Fig. 4a). The suggestion that SPRs increase with erosion rate for a given soil thickness becomes strongly corroborated by a global compilation of published soil production numbers where catchment mean erosion rates were also measured (Fig. 4b). These data show that point SPRs under average soil thickness tend to match catchment mean erosion rates, and that there is a positive correlation between SP_{\max} and catchment mean erosion rate. Given the uncertainty associated with the estimates of SP_{\max} for the SGM, these observations are most strongly supported by previously published data, although the correlation is noted here for the first time. New data from the SGM do, however, strongly demonstrate that SPRs increase well beyond 'background' values in landslide-dominated areas: most soil production numbers under thin soils in these areas exceed the

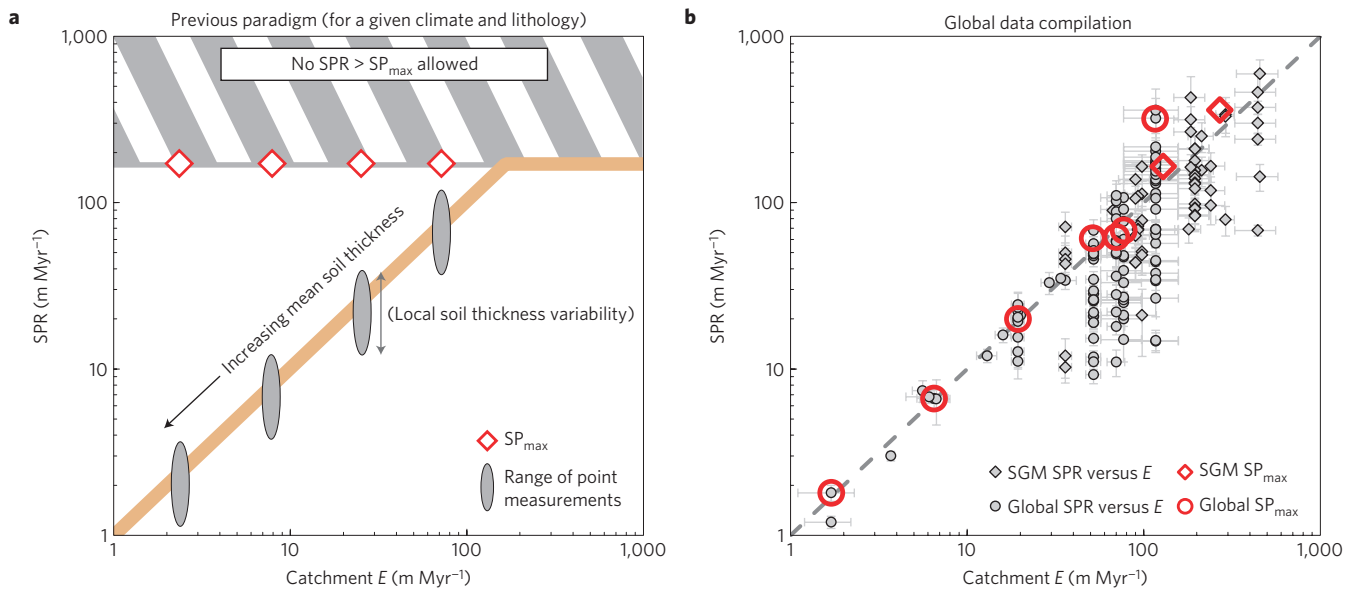


Figure 4 | Soil production versus erosion rates. **a**, Concept figure illustrating entrenched paradigm inconsistent with data. **b**, Global compilation of ^{10}Be -based SPRs from studies also quantifying ^{10}Be catchment-averaged erosion rates. Black outlined grey symbols are individual point measurements, and red open symbols indicate SP_{max} where soil-production function was quantified (from low to high: northern Chile; northern Australia; southeastern Australia; Tennessee Valley, California; Point Reyes, California; Oregon Coast Range; SGM gentle; SGM steep). Dashed line is 1:1 for reference. See Supplementary Information for additional study references.

background rate implied by the soil-production function defined in more slowly eroding parts of the landscape (Figs 3 and 4a). If our interpretation is correct, there are some intriguing implications.

First, if SP_{max} does indeed increase with erosion rate, this would imply a more extensive soil cover than predicted by our modelling exercise (Fig. 2b). Second, the SPR data may help explain why neither Binnie *et al.*¹⁵ nor DiBiase *et al.*¹⁰ observed the drainage-area dependence of catchment-averaged erosion rates in landslide-prone areas that is predicted by models based on a background erosion rate set by a fixed soil-production function and assumed SP_{max} (refs 11,23). Third, the increase in SP_{max} shown by our data would imply an interesting feedback between tectonically driven erosion rates and processes mobilizing sediment across hillslopes. Specifically, the exponential decrease in SPR with increasing soil thickness has long been attributed to a decline in the frequency at which the soil-rock interface is disturbed by physical weathering processes including bioturbation^{4,20,25}. By analogy, we reason that the systematic increase of soil production with total erosion rate observed here reflects an increase in the frequency of disturbance for a given soil thickness. Such feedbacks are reasonably clear for landsliding, but are difficult to resolve for the biogenically driven soil production processes, except perhaps tree throw, and should be pursued in future studies. Finally, chemical weathering increases with erosion^{26,27} and is likely to contribute significantly to increasing soil production, but has yet to be fully quantified for such rugged topography. We suggest that dynamic coupling between chemical weathering and the increase of SP_{max} with erosion leads to enhanced persistence of soils, and, therefore, the transition to bedrock landscapes is not abrupt.

Methods

REI. We observe that extreme values of slope and curvature correspond with bedrock outcrops, which tend to be blocky, fractured masses protruding significantly from the surrounding slopes. For each of our detrital CRN sample basins lying within the extent of the LiDAR data set (Fig. 1a), we use the dip of a 3×3 cell plane to determine local slope from the 1 m resolution DEM. We calculated a REI based on the percentage of cells within a given area greater than a critical slope, S^* . For eight calibration patches (~ 1 ha each), we calculated REI for several S^* values and compared the values to independently mapped rock using surface-normal, high-resolution (~ 1 cm) panoramic photographs²². REI is,

therefore, interpreted as a direct proxy for the percentage of exposed bedrock within a given area. The strongest linear correlation between REI and the percentage of exposed rock mapped was for $S^* = 45^\circ$ ($R^2 = 0.99$). A more detailed analysis of the methodology can be found in ref. 22.

Landslide model. Yanites *et al.*¹¹ developed a two-dimensional model that combined representations of slow background erosion, stochastic landsliding and *in situ* cosmogenic ^{10}Be production, to evaluate the influence of landslides on perceived detrital CRN erosion rates. We adapt and simplify this model to explore the dependence of soil cover on erosion rate. Abstracting the landscape as a 10 m resolution, 5 km by 5 km grid, we step through time at 0.5 year intervals, generating landslides at random locations using a Poisson distribution of recurrence intervals. Landslide areal extent is assumed to follow a bounded power-law distribution, using scaling parameters (including the area-depth relationship) estimated by Lavé and Burbank²⁴. We ran the model for 10^5 years to ensure reaching steady state, and calculate the time at each cell since the last landslide. We assume that 1,000 years is sufficient time to develop a SGM soil, on the basis of rough estimates of colluvial soil growth, and calculate the fraction of bedrock as the number of cells 'younger' than 1,000 years divided by the total number of cells. We evaluate the change in soil cover with erosion rate by changing the mean recurrence interval of the Poisson distribution (controls landsliding frequency) and assuming the size distribution of landslides stays constant. See Supplementary Fig. S2 for example output.

SPRs. Fifty-eight samples of in-place bedrock or saprolite were collected from beneath colluvial soils (depth, H) or flush with ground surface (0 depth). We isolated quartz from these samples and from fluvial sand collected from channels following standard procedures for ^{10}Be analyses. Application of CRNs to understanding landscapes is extensively reviewed^{26,28–30} and is only summarized here. *In situ*-produced CRNs are used extensively to quantify bedrock erosion^{4,25,28,29}, soil-production^{4,20,25} and spatially averaged erosion rates^{10,11,14–16,22,25,30}. CRN concentrations accumulate in materials at or near the Earth's surface as cosmic rays bombard atoms, such as Si and O in quartz and other minerals in rock and sediments. We extracted ^{10}Be using cation-exchange chemistry and measured concentrations with standard protocols at PRIME and LLNL laboratories. ^{10}Be -production rates in quartz are based on the sea level and high latitude rate of $5.1 \text{ atoms g}^{-1} \text{ yr}^{-1}$ and were corrected for latitude and altitude effects as well as for the slope and depth shielding of every sample. We measure concentrations of only ^{10}Be because sample exposure history is young enough to preclude measuring ^{26}Al to test for steady-state erosional processes³⁰. The CRONUS-Earth online calculator is updated to determine latitude-altitude-corrected production rates²⁸ (<http://hess.ess.washington.edu/math>) and we used ^{10}Be -production rates from the calculator with our measured ^{10}Be concentrations and pixel-by-pixel shielding corrections to quantify catchment-averaged erosion rates³⁰ and point-specific SPRs (ref. 4).

Received 10 March 2011; accepted 30 December 2011;
published online 5 February 2012

References

- Ahnert, F. Brief description of a comprehensive three-dimensional process-response model of landform development. *Z. Geomorph. N. F.* **25**, 29–49 (1976).
- Anderson, R. S. & Humphrey, N. F. in *Quantitative Dynamic Stratigraphy* (ed. Cross, T. A.) 349–361 (Prentice-Hall, 1989).
- Carson, M. & Kirkby, M. *Hillslope Form and Process* (Cambridge Univ. Press, 1972).
- Heimsath, A. M., Dietrich, W. E., Nishiizumi, K. & Finkel, R. C. The soil production function and landscape equilibrium. *Nature* **388**, 358–361 (1997).
- Larsen, I. J., Montgomery, D. R. & Korup, O. Landslide erosion controlled by hillslope material. *Nature Geosci.* **3**, 247–251 (2010).
- Tucker, G. E. & Hancock, G. R. Modelling landscape evolution. *Earth Surf. Process. Landf.* **35**, 28–50 (2010).
- Pelletier, J. D. & Rasmussen, C. Quantifying the climatic and tectonic controls on hillslope steepness and erosion rate. *Lithosphere* **1**, 73–80 (2009).
- Dietrich, W. E. *et al.* in *Prediction in Geomorphology* Vol. 135 (eds Wilcock, Peter R. & Iverson, R.) 103–132 (Geophysical Monograph Series, AGU, 2003).
- Brantley, S. L. *et al.* *Frontiers in Exploration of the Critical Zone: Report of a workshop sponsored by the National Science Foundation (NSF). October 24–26, 2005, Newark, Delaware* (2006).
- DiBiase, R. A., Whipple, K. X., Heimsath, A. M. & Ouimet, W. B. Landscape form and millennial erosion rates in the San Gabriel Mountains, CA. *Earth Planet. Sci. Lett.* **289**, 134–144 (2010).
- Yanites, B. J., Tucker, G. E. & Anderson, R. S. Numerical and analytical models of cosmogenic radionuclide dynamics in landslide-dominated drainage basins. *J. Geophys. Res.* **114**, F01007 (2009).
- Spotila, J. A., House, M. A., Blythe, A. E., Niemi, N. A. & Bank, G. C. Controls on the erosion and geomorphic evolution of the San Bernardino and San Gabriel Mountains, southern California. *Geol. Soc. Am. Spec. Pap.* **365**, 205–230 (2002).
- Peterson, M. D. & Wesnousky, S. G. Fault slip rates and earthquake histories for active faults in Southern California. *Bull. Seismol. Soc. Am.* **84**, 1608–1649 (1994).
- Ouimet, W. B., Whipple, K. X. & Granger, D. E. Beyond threshold hillslopes: Channel adjustment to baselevel fall in tectonically active mountain ranges. *Geology* **37**, 579–582 (2009).
- Binnie, S. A., Phillips, W. M., Summerfield, M. A. & Fifield, L. K. Tectonic uplift, threshold hillslopes, and denudation rates in a developing mountain range. *Geology* **35**, 743–746 (2007).
- Norton, K., von Blanckenburg, F. & Kubik, P. Cosmogenic nuclide-derived rates of diffusive and episodic erosion in the glacially sculpted upper Rhone Valley, Swiss Alps. *Earth Surf. Process. Landf.* **35**, 651–662 (2010).
- Schmidt, K. M. & Montgomery, D. R. Limits to relief. *Science* **270**, 617–620 (1995).
- Strahler, A. N. Equilibrium theory of erosional slopes approached by frequency distribution analysis. *Am. J. Sci.* **248**, 673–696; 800–814 (1950).
- Burbank, D. W. *et al.* Bedrock incision, rock uplift and threshold hillslopes in the Northwestern Himalayas. *Nature* **379**, 505–510 (1996).
- Heimsath, A. M. Eroding the land: Steady-state and stochastic rates and processes through a cosmogenic lens. *Geol. Soc. Am. Spec. Pap.* **415**, 111–129 (2006).
- Roering, J. J., Kirchner, J. W. & Dietrich, W. E. Hillslope evolution by nonlinear, slope-dependent transport: Steady state morphology and equilibrium adjustment timescales. *J. Geophys. Res.* **106**, 16499–16513 (2001).
- DiBiase, R. A., Heimsath, A. M. & Whipple, K. X. Hillslope response to tectonic forcing in threshold landscapes. <http://dx.doi.org/10.1002/esp.3205> (2012).
- Niemi, N. A., Oskin, M., Burbank, D. W., Heimsath, A. J. M. & Gabet, E. J. Effects of bedrock landslides on cosmogenically determined erosion rates. *Earth Planet. Sci. Lett.* **237**, 480–498 (2005).
- Lavé, J. & Burbank, D. W. Denudation processes and rates in the Transverse Ranges, southern California: Erosional response of a transitional landscape to external and anthropogenic forcing. *J. Geophys. Res.* **109**, F01006 (2004).
- Heimsath, A. M., Chappell, J. & Fifield, K. Eroding Australia: Rates and processes from Bega Valley to Arnhem Land. *Geol. Soc. Lond. Spec. Publ.* **346**, 225–241 (2010).
- von Blanckenburg, F. The control mechanisms of erosion and weathering at basin scale from cosmogenic nuclides in river sediment. *Earth Planet. Sci. Lett.* **242**, 223–239 (2006).
- Dixon, J. L., Heimsath, A. & Amundson, R. The critical role of saprolite weathering and climate in landscape evolution. *Earth Surf. Process. Landf.* **34**, 1507–1521 (2009).
- Balco, G., Stone, J. O., Lifton, N. A. & Dunai, T. J. A complete and easily accessible means of calculating surface exposure ages or erosion rates from ^{10}Be and ^{26}Al measurements. *Quat. Geochronol.* **3**, 174–195 (2008).
- Gosse, J. C. & Phillips, F. M. Terrestrial in situ cosmogenic nuclides: theory and application. *Quat. Sci. Rev.* **20**, 1475–1560 (2001).
- Bierman, P. R. Rock to sediment—Slope to sea with Be-10—Rates of landscape change. *Annu. Rev. Earth Planet. Sci.* **32**, 215–255 (2004).

Acknowledgements

W.E. Dietrich helped A.M.H. collect the first SGM samples and sowed the concept of 'bionic gophers'. Numerous graduate students assisted in sample collection and stimulating discussions on this work. NSF Geomorphology and Land Use Dynamics financially supported it. Laser altimetry was acquired and processed by NCALM with support from ASU and Caltech. A thoughtful review by G. Tucker improved the manuscript.

Author contributions

All authors conducted field work, contributed to the experimental design and writing of this manuscript. A.M.H. carried out CRN chemical analyses; A.M.H. and R.A.D. analysed the CRN data.

Additional information

The authors declare no competing financial interests. Supplementary information accompanies this paper on www.nature.com/naturegeoscience. Reprints and permissions information is available online at <http://www.nature.com/reprints>. Correspondence and requests for materials should be addressed to A.M.H.

Soil production limits and the transition to bedrock-dominated landscapes

Arjun M. Heimsath, Roman A. DiBiase, Kelin X. Whipple

Soil Production Rate Determination

Sample Site Selection:

Differences in the erosional processes dominant on soil-mantled and bedrock-dominated landscapes are critical to consider when applying CRN methodology to landscapes like the San Gabriel Mountains. Specifically, to use ^{10}Be concentrations to quantify soil production rates, we must assume that the overlying soil thickness at any given sample location is temporally constant (Heimsath et al., 1997). While this assumption is reasonably well supported for smooth, soil-mantled landscapes (Heimsath et al., 2000), it is not likely to be applicable to soil mantled landscapes eroding by stochastic processes such as shallow landsliding or infrequent catastrophic events (Heimsath, 2006). We selected sampling sites cautiously to avoid the potential for periodic soil stripping events (Lavé and Burbank, 2004) on the side slopes of the rapidly eroding catchments where slopes approached, but did not exceed, threshold values (about 32°). In the catchments where slopes were at threshold values or greater we focused our sampling efforts on the ridge crests or slopes where bedrock was continuous with the slope morphology or mantled with a thin layer of soil. We deliberately avoided samples from areas where the steady-state soil depth assumption could not be applied, or where episodic or catastrophic soil stripping processes were readily apparent. We did not collect any samples from tors or bedrock fins that are likely to be out of local steady state due to the fact that they are sticking up out of ground and are therefore likely to be eroding more slowly than the surrounding ground surface (Heimsath et al., 2000).

Two examples of such smoothly convex-up soil mantled parts of a rapidly eroding landscape are shown in Fig. S1. In both cases, the sample locations are representative of the locally continuous, albeit thin, soil mantle. Samples collected from the in-place saprolite from beneath the colluvial soil yielded low ^{10}Be concentrations, thus high soil production rates (Table S1). Importantly, if these sample locations were impacted by the landsliding that is evident in other parts of the catchments, there would be some morphological evidence of such episodic events. Specifically, a landslide removing the underlying bedrock beneath the shallow soil mantle, as well as the soil, would leave a locally concave-up feature behind on the hillslope that would be readily visible. Such features take

time to “heal” and we address below the timescale of ^{10}Be accumulation for such sample locations if such events were to have ever occurred for one of our sample locations.

Accumulation of in situ produced ^{10}Be

Thin soils shield the underlying saprolite or bedrock relatively little (Dunai, 2000)(Table S1). If only soil is periodically stripped away by shallow landsliding, the impact on the ^{10}Be concentrations in the underlying saprolite is small, on the order of 10-25 %. Conversely, the impact on ^{10}Be concentrations in the saprolite can be quite significant under episodic landsliding that removes over a meter of saprolite containing the ^{10}Be that we measure to determine soil production rates. The potential impact of such landslides on the interpreted soil production rates was fully explored by Heimsath (2006). In summary of that modeling work, the only way to impact the ^{10}Be -based soil production rates significantly is to remove bedrock, which would leave a morphological signature. The time scale of such signatures to “heal” depends on the local topography and (1) how quickly soil can “refill” the hole from uphill and surrounding landscape, and (2) the soil production rate in the freshly exposed landslide scar. Of course, because such scars create locally convergent areas in the landscape they are likely to expand in size due to positive feedbacks and increased erosion due to overland flow processes. Scars are, therefore, not likely to “heal” quickly in the context of such environments and the absence of scars is considered a reasonable indicator of local steady state for a continuous soil mantle.

Given both the morphological characteristics of our sample sites and the simple estimate for potential landslide impacts, we interpret the high soil production rate measurements to be robust. Another potential source of artifact in the soil production rate computation is the correction applied by the overlying soil shielding. Specifically, concentrations of ^{10}Be used to compute these soil production rates are relatively low and are not significantly corrected by the shielding depth correction (Table S1): calculated soil production rates are, therefore, high irrespective of any depth-correction. In fact, an artifactual relationship between soil production and depth would have a slope of about -0.01 (equal to the field soil bulk density of 1.4 g cm^{-3} divided by the mean attenuation length for cosmic rays, 165 g cm^{-2}). The slopes of the variance-weighted best fits to the soil production rate versus soil depth data are -0.03 for both the high and low slope samples, and are statistically different from a potential artifact due to shielding correction.

Soil Production Rate Versus Average Erosion Rate

Very few studies have quantified soil production rates and basin averaged erosion rates for the same landscape. We compiled data from studies that used in situ produced ^{10}Be concentrations for **both** the soil production rate quantification and the average erosion rate measurement. These regions where both soil production and average erosion rates were defined are, from low to high: northern Chile (Owen et al., 2011); central Australia (Heimsath et al., 2010); northern Australia (Heimsath et al., 2009); southeastern Australia (Heimsath et al., 2000); Tennessee Valley, CA (Heimsath et al., 1997); Point Reyes, CA (Heimsath et al., 2005); Oregon Coast Range (Heimsath et al., 2001b); this study gentle ($< 30^\circ$); this study steep ($> 30^\circ$). For all but the two most slowly eroding landscapes, there was an observed spatial variation of soil depths across the landscape. The soil production rates from beneath thick soils lie beneath the 1:1 line of Fig. 4b. In each case it is not reasonable to take the average of these rates and equate that to the basin-averaged erosion rate because the spatial distribution of soil depths was not quantified.

To make a direct comparison with between an “average soil production rate” and the average erosion rate determined for a catchment a significantly more extensive data set is required (Heimsath et al., 2001a). The Heimsath et al. (2001a) study is the only study that we know of that attempted such a comparison, and it was done for an unchanneled catchment only slightly larger than 1 hectare. In that study, 17 point samples of ^{10}Be (and ^{26}Al)-derived soil production and bedrock erosion rates were combined with over 100 measurements of soil thickness to produce a meter-scale map of soil thickness and, by using the soil production function, soil production rate. This high-resolution map of soil production rate was then used to numerically determine an average soil production rate for the small catchment, which was compared to the single detrital sample collected from the mouth of the basin for a ^{10}Be -derived average erosion rate for the small catchment. These rates were also compared to the average erosion rate determined for the larger drainage basin by detrital samples as well as bedrock strath samples in the main river. In that study case alone the comparison between an average soil production rate and a catchment-averaged erosion rate is valid given the spatial extent of the data collected.

Landslide Model

One of the key observations we make in the SGM is the presence of extensive, though patchy soil cover in rapidly eroding catchments with threshold slopes. Under the existing paradigm,

catchments with $E > SP_{\max}$ are predicted to lose their soil mantle, and hillslopes maintain equilibrium with channel incision by landsliding at a rate of $E_L = E - SPR$. In real landscapes, however, soil thickness and local erosion rates vary even in gentle, soil-mantled catchments interpreted to be at steady state (grey ovals, Fig. 4a). In steep, landslide-affected catchments this variability is even starker; intermittent landslide events expose bedrock that then slowly regrows a soil until the next landslide occurs. Such a landscape might be expected to resemble a patchwork of thin, variable soils and bare landslide scars. The detail of how percent soil cover varies with total erosion rate depends on the spatial and temporal distribution of landslides, as well as the timescale for soil formation on steep slopes.

To address this issue, we take advantage of a 2-D numerical landslide model developed by Yanites et al. (2009) for estimating the influence of landsliding on detrital CRN erosion rates. We simplify this model to evaluate only the spatial distribution of the time since the last landslide (Fig. S2). The size distribution of landslides follows the power-law scaling parameters estimated for the SGM by Lavé and Burbank (2004). We then tune the frequency of landslides so that $E_L = E - SPR$. We choose a timescale for colluvial soil generation to be 1000 years, but emphasize that this is only a rough estimate – the precise rate of soil regrowth on steep hillslopes depends on the soil production function, as well as the “background” steady state soil production rate, SPR , which must be less than SP_{\max} in order to grow and retain a soil. Because landslides are deep compared to biogenic-related soil production, relatively few landslides are required to achieve the fluxes required by E_L in the SGM (Figs. 2a, S2). The result of this simple exercise is that the presence of soils on steep landscapes does not necessarily require high rates of soil production. Indeed, what we are proposing instead is that the transition to landsliding and threshold slopes is unrelated to SP_{\max} , and arises independent of the limits of soil production, which appear to vary with erosion rate.

Supplementary Information References

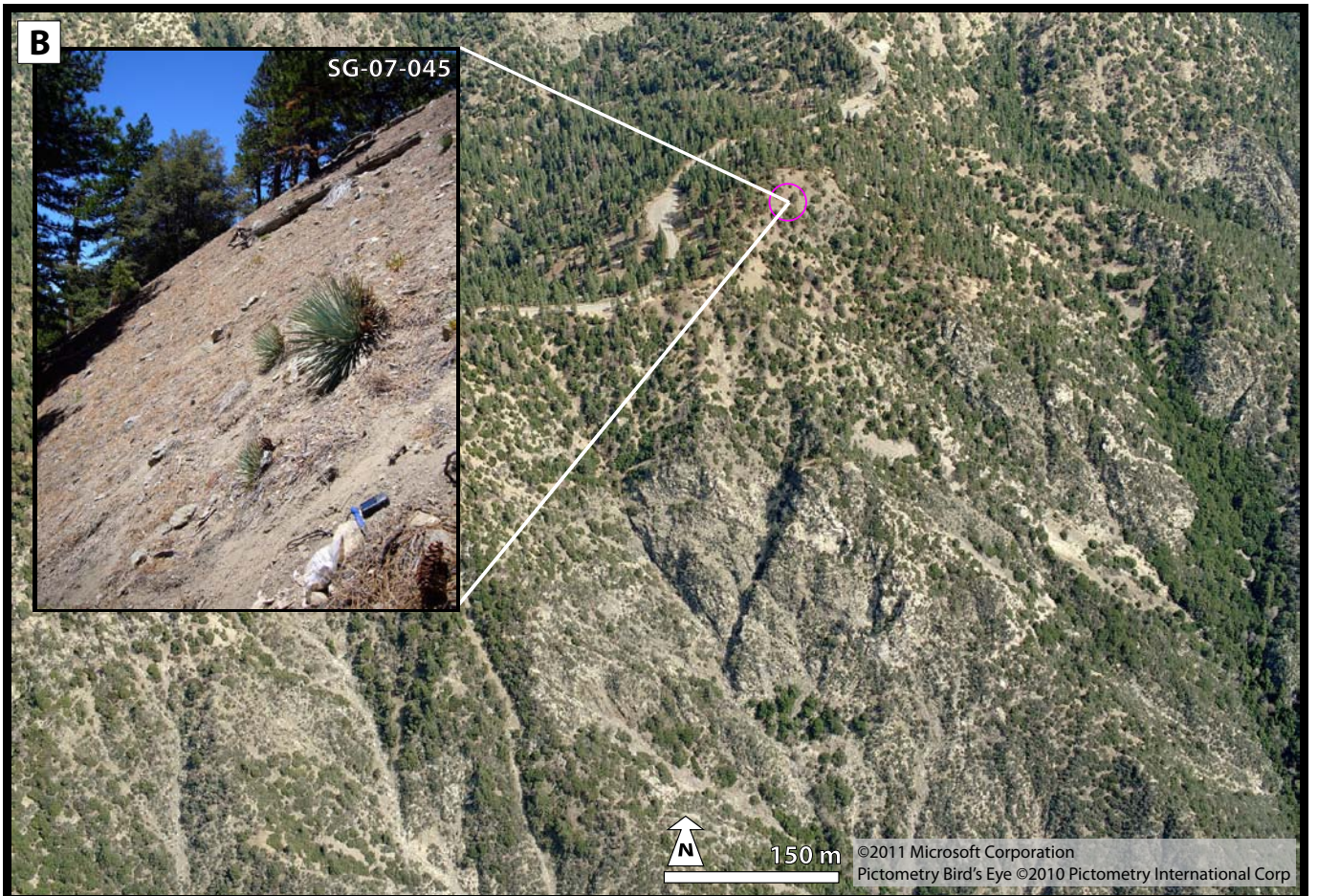
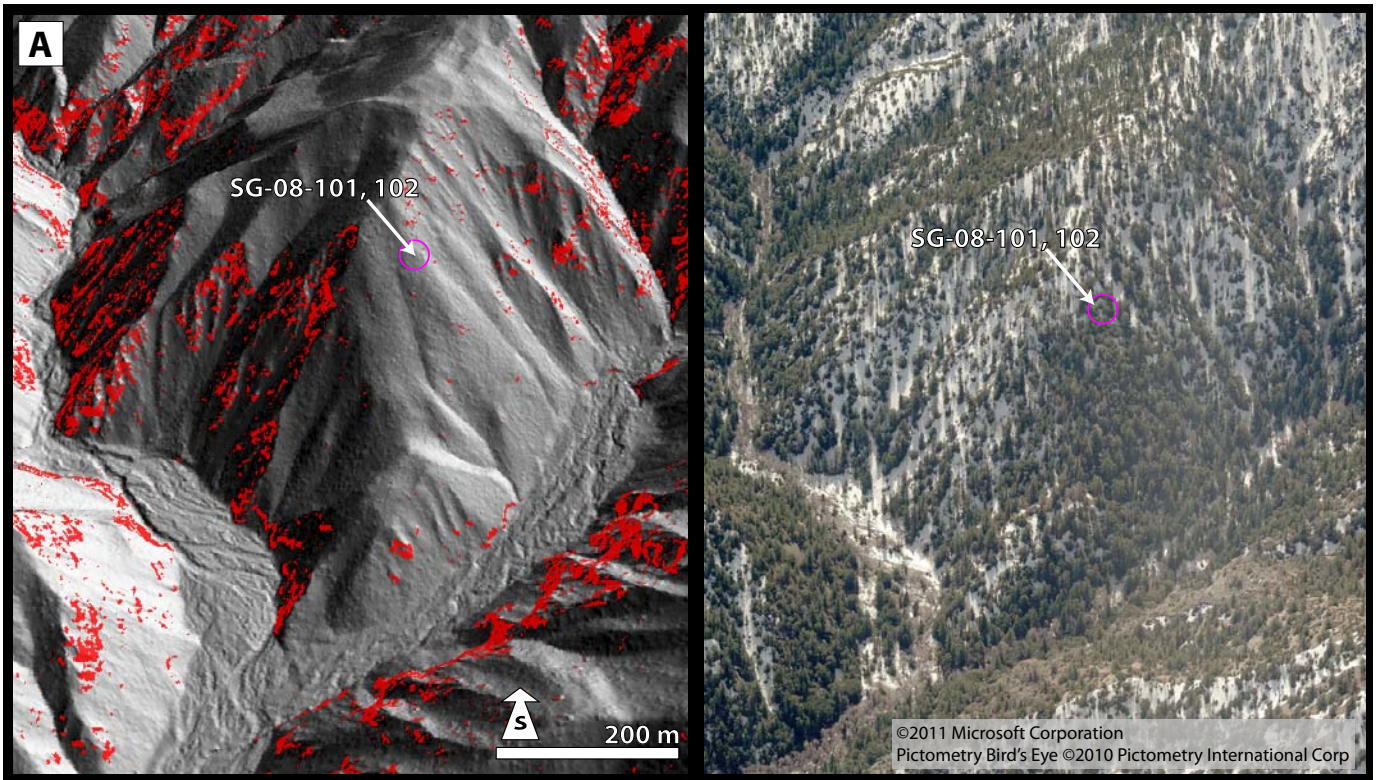
- Balco, G., Stone, J.O., Lifton, N.A., and Dunai, T.J., 2008, A complete and easily accessible means of calculating surface exposure ages or erosion rates from Be-10 and Al-26 measurements: *Quaternary Geochronology*, v. 3, p. 174-195.
- Dunai, T.J., 2000, Scaling factors for production rates of in situ produced cosmogenic nuclides: a critical reevaluation: *Earth and Planetary Science Letters*, v. 176, p. 157-169.
- Heimsath, A.M., 2006, Eroding the land: Steady-state and stochastic rates and processes through a cosmogenic lens: *Geological Society of America Special Paper*, v. 415, p. 111-129.
- Heimsath, A.M., Chappell, J., Dietrich, W.E., Nishiizumi, K., and Finkel, R.C., 2000, Soil production on a retreating escarpment in southeastern Australia: *Geology*, v. 28, p. 787-790.

- , 2001a, Late Quaternary erosion in southeastern Australia: a field example using cosmogenic nuclides: *Quaternary International*, v. 83-85, p. 169-185.
- Heimsath, A.M., Chappell, J., and Fifield, K., 2010, *Eroding Australia: rates and processes from Bega Valley to Arnhem Land*: Geological Society, London, Special Publications, v. 346, p. 225-241.
- Heimsath, A.M., Dietrich, W.E., Nishiizumi, K., and Finkel, R.C., 1997, The soil production function and landscape equilibrium: *Nature*, v. 388, p. 358-361.
- , 2001b, Stochastic processes of soil production and transport: erosion rates, topographic variation, and cosmogenic nuclides in the Oregon Coast Range: *Earth Surface Processes and Landforms*, v. 26, p. 531-552.
- Heimsath, A.M., Fink, D., and Hancock, G.R., 2009, The 'humped' soil production function: eroding Arnhem Land, Australia: *Earth Surface Processes and Landforms*, v. 34, p. 1674-1684.
- Heimsath, A.M., Furbish, D.J., and Dietrich, W.E., 2005, The illusion of diffusion: Field evidence for depth-dependent sediment transport: *Geology*, v. 33, p. 949-952.
- Lavé, J., and Burbank, D.W., 2004, Denudation processes and rates in the Transverse Ranges, southern California: Erosional response of a transitional landscape to external and anthropogenic forcing: *Journal of Geophysical Research*, v. 109, p. doi:10.1029/2003JF000023.
- Owen, J.J., Amundson, R., Dietrich, W.E., Nishiizumi, K., Sutter, B., and Chong, G., 2011, The sensitivity of hillslope bedrock erosion to precipitation: *Earth Surface Processes & Landforms*, v. 36, p. 117-135.
- Yanites, B.J., Tucker, G.E., and Anderson, R.S., 2009, Numerical and analytical models of cosmogenic radionuclide dynamics in landslide-dominated drainage basins: *Journal of Geophysical Research*, v. 114, p. doi:10.1029/2008JF001088.

Supplementary Information Figure Captions

Figure S1. Contextual images showing location of three high SPR samples. **(a)** Samples SG-08-101 (SPR = 338 m/Ma) and SG-08-102 (SPR = 329 m/Ma) lie on a smooth, divergent nose, devoid of exposed rock as expressed in both LiDAR-derived hillshade image (left) and oblique aerial imagery (right, same view). Red pixels on left image highlight areas where $S^* > 45^\circ$ and are therefore included in the REI calculation. **(b)** Sample SG-07-045 (SPR = 594 m/Ma) is situated on a steep (45 degrees), but smooth and divergent hillslope (inset photo shows sample location in foreground) interpreted to be unaffected by recent mass wasting events visible in oblique aerial imagery.

Figure S2. Examples of landslide model runs that helped generate Fig. 2a, showing spatial extent of time since last landslide. We interpret yellow areas (older than 1000 years) to be soil-mantled. The total erosion rate (E) is equal to the landsliding erosion rate (E_l) added to a fixed soil production rate of 200 m/Ma. Each square is 5 km x 5 km in dimension.



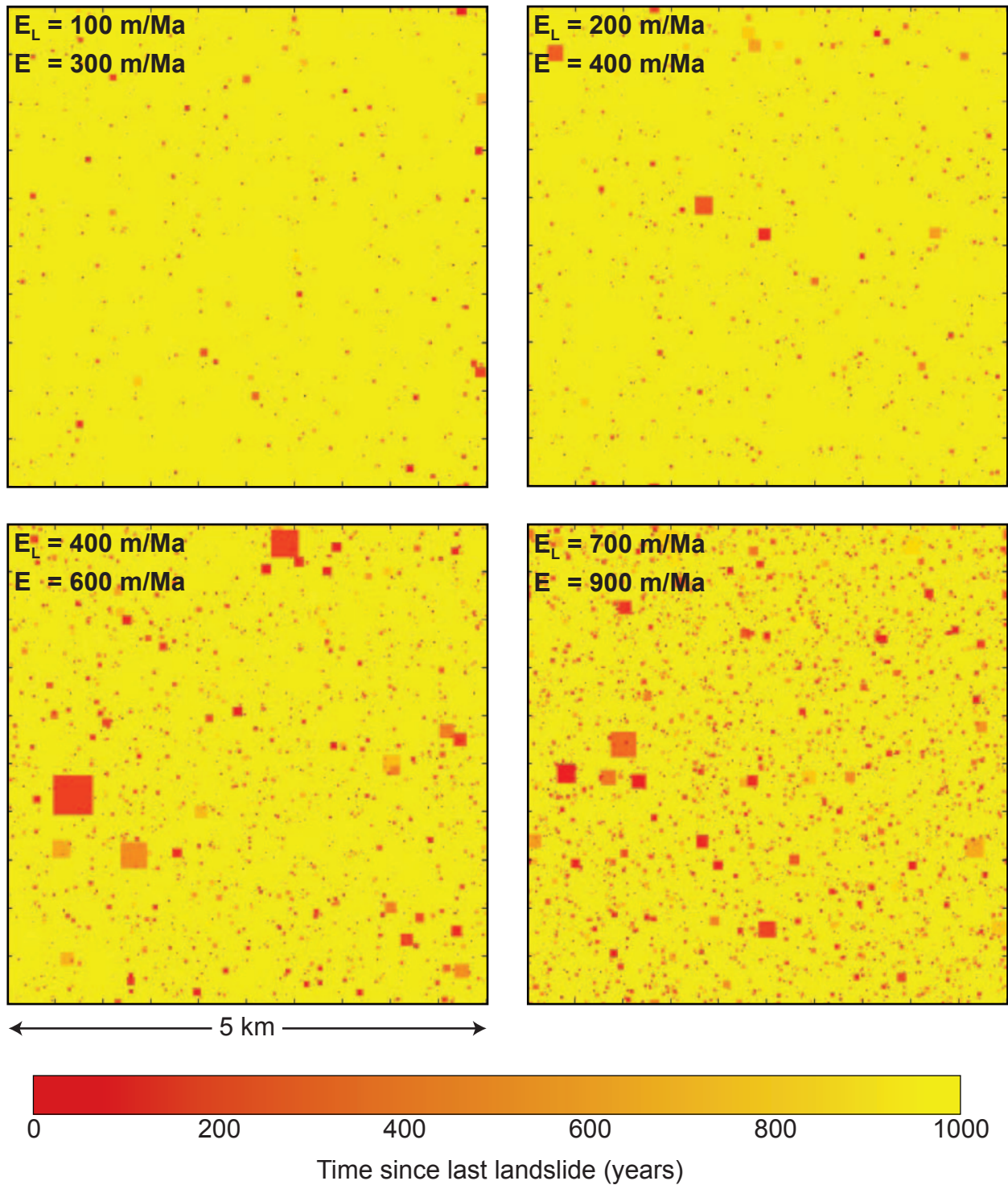


figure S2

TABLE S1: SOIL PRODUCTION AND AVERAGE EROSION RATES FROM COSMOGENIC BE-10 CONCENTRATIONS

Sample	Weight (g)	Carrier (µg)	Latitude (DD)	Longitude (DD)	Elevation (m)	Depth (cm)	Local Slope (degrees)	Avg. Slope (degrees)	H-slope* correction	[Be-10] atoms g ⁻¹	error	SPR (m Ma ⁻¹)	error
SG-1	138.46	403	34.2090	-117.7714	1072	0	31	30	0.97	24812	2526	300	38
SG-2	100.72	458	34.2118	-117.7685	1072	0	30	30	0.97	31884	1397	240	19
SG-6	72.21	407	34.1868	-117.7632	947	0	12	35	0.93	15606	4515	460	148
SG-7	143.65	461	34.1856	-117.7662	950	5	35	35	0.87	19234	1200	373	34
SG-10	145.71	459	34.207	-117.7621	855	38	0	18	0.75	96379	2945	68	5
SG-101	60.95	385	34.2852	-118.1519	1673	0	0	35	1.00	89138	6078	156	32
SG-102	97.33	382	34.2852	-118.1519	1673	30	0	35	0.75	42231	1518	251	51
SG-103	87.73	377	34.3717	-118.0710	2015	23	0	26	0.78	169007	8781	78	17
SG-104	85.78	379	34.3717	-118.0710	2015	30	0	26	0.75	773360	406132	21	9
SG-105	71.98	377	34.3707	-118.0701	2005	43	20	26	0.62	215144	10047	48	12
SG-106	4.15	367	34.3706	-118.0692	1990	36	25	26	0.64	209929	13146	51	13
SG-107	67.69	373	34.3569	-118.0631	1804	15	33	26	0.95	87295	2481	164	29
SG-108	104.44	383	34.3543	-118.0580	1625	15	37	26	0.94	112041	7431	113	23
SG-110	71.08	387	34.2931	-118.0199	1725	10	0	26	0.92	124135	4809	106	20
SG-111	77.68	377	34.2930	-118.0202	1721	44	14	26	0.58	130184	4427	63	15
SG-112	60.70	379	34.2932	-118.0211	1729	27	0	26	0.74	238056	11651	44	9
SG-113	76.27	382	34.2908	-118.0218	1650	34	25	26	0.67	207673	9994	44	10
SG-115	36.67	379	34.2832	-118.0263	1390	10	0	15	0.90	77036	7822	138	33
SG-153	53.63	383	34.3273	-117.7998	2194	20	18	29	0.83	173488	7192	90	18
SG-154	50.71	387	34.3460	-118.0060	1800	44	12	12	0.62	212347	8250	43	10
SG-155	72.64	383	34.3469	-118.0059	1790	54	10	12	0.58	171194	8059	50	13
SG-156	18.69	384	34.3476	-118.0061	1780	45	17	12	0.60	679503	15236	12	3
SG-200	49.20	380	34.3586	-117.9922	1710	16	0	13	0.95	195283	6867	68	13
SG-201	92.73	383	34.3589	-117.9920	1710	10	15	13	0.95	190834	6398	69	13
SG-202	60.19	383	34.3590	-117.9922	1706	15	20	13	0.95	183671	6204	72	13
SG-203	67.25	382	34.3592	-117.9923	1702	10	25	13	0.95	123053	3774	109	20
SG-07-009	47.91	372	34.3215	-118.0866	1132	28	0	15	0.76	144389	4764	69	12
SG-07-011	63.11	376	34.3320	-117.9483	2137	12	17	24	0.86	167501	4979	93	18
SG-07-012	117.83	377	34.3318	-117.9481	2128	20	20	24	0.78	166903	3965	84	17
SG-07-013	98.04	375	34.3318	-117.9481	2120	20	0	24	0.82	121937	3336	121	24
SG-07-014	89.31	379	34.3318	-117.9481	2115	24	14	24	0.79	91160	3372	156	32
SG-07-015	71.88	381	34.3259	-117.9517	1897	0	20	24	0.98	111474	4066	139	26
SG-07-016	92.75	372	34.3276	-117.9507	1965	0	10	24	0.99	126271	6090	130	25
SG-07-017	80.69	377	34.3304	-117.9498	2068	0	22	24	0.98	116709	4554	147	28
SG-07-019	34.94	376	34.3484	-118.0045	1773	49	5	12	0.64	875243	20851	10	2
SG-07-020	12.92	358	34.3482	-118.0035	1785	50	17	12	0.60	194067	10544	46	12
SG-07-021	17.96	347	34.3471	-118.0030	1802	35	0	12	0.68	142209	7458	71	16
SG-07-023	3.23	355	34.3627	-117.9108	1958	25	0	31	0.80	31277	5388	427	145
SG-07-024	73.47	373	34.3615	-117.9107	1912	5	35	31	0.87	44831	1899	315	61
SG-07-025	42.52	375	34.3614	-117.9110	1889	7	35	31	0.87	52156	2518	266	54
SG-07-031	67.81	383	34.3348	-117.9695	1973	13	0	21	0.88	69810	2692	210	41
SG-07-032	72.70	379	34.3348	-117.9695	1973	3	0	21	1.00	79523	2678	210	38
SG-07-033	75.87	391	34.3348	-117.9695	1973	20	12	21	0.80	143406	4663	92	18
SG-07-034	92.21	380	34.3348	-117.9695	1973	5	12	21	0.99	124486	5886	132	25
SG-07-035	46.93	376	34.3264	-117.9690	1703	3	30	21	0.97	94629	4582	146	28
SG-07-038	98.42	378	34.3307	-117.9700	1847	3	27	21	0.97	84063	3061	178	33
SG-07-041	44.68	376	34.3307	-117.9700	1840	12	0	21	0.90	183575	6055	83	15
SG-07-042	96.16	379	34.3307	-117.9700	1835	12	0	21	0.90	155283	5968	98	18
SG-07-044	75.78	373	34.3524	-117.8792	2077	0	0	23	1.00	123129	4471	143	26
SG-07-045	58.68	364	34.3521	-117.8791	2058	8	45	38	0.83	29193	2350	594	125
SG-08-100	43.02	309	34.3639	-117.8379	1934	25	0	31	0.98	168775	6861	79	16
SG-08-101	30.12	305	34.3648	-117.8383	1880	8	40	31	0.75	35367	3537	338	90
SG-08-102	29.96	305	34.3648	-117.8383	1880	10	40	31	0.90	43445	2879	329	69
SG-08-105	30.07	308	34.3712	-117.8581	2494	0	0	35	1.00	231741	26038	96	23
SG-08-106	30.18	307	34.3714	-117.8578	2491	0	0	35	1.00	189159	14059	118	25
SG-08-108	66.34	309	34.3720	-117.8571	2442	20	35	35	0.80	105570	3844	166	34
SG-08-110	30.03	305	34.3723	-117.8631	2398	5	15	32	0.98	127553	6192	163	31
New Basin Sediment Samples									N(z,I)			Avg. E	
SG-08-03	51.5	308	34.3720	-117.8356	-	-	-	-	4.20	46340	5210	293	48
SG-08-04	54.09	312	34.3697	-117.8359	-	-	-	-	4.35	28510	5011	493	111
SG-08-05	53.77	309	34.3692	-117.8383	-	-	-	-	3.88	36661	4393	343	58
SG-08-09	59.99	305	34.3857	-117.8245	-	-	-	-	4.02	29969	2610	434	59

Concentration errors include 1 σ from AMS. All errors propagated to SPR: erosion or soil production rates.

N(z,I) is the latitude and altitude production rate scaling factor used here only for catchment-averaged rates (Dunai, 2000).

Densities: Soil, 1.4 g cm⁻³, for H correction; Sediment, 2.6 g cm⁻³, for Avg. E; Point samples, 2.0-2.6 g cm⁻³, for soil production; lambda 165 g cm⁻².

¹⁰Be from rescaled sea level production rate of and 5.1 atoms g⁻¹ yr⁻¹ (Balco et al., 2008); ¹⁰Be ratios calibrated to 07KNSTD, measured at PRIME lab AMS.

Local slope measured for point samples. Average slope measured for local patches and used to distinguish between high and low soil production functions.

*H-slope factor corrected nuclide production rate for soil depth and local slope shielding for individual sample locations (Heimsath et al., 1997; 2006).